Kinetic simulation of capacitively coupled plasmas driven by trapezoidal asymmetric voltage pulses

Paola Diomede[a] and Demetre J. Economou[b]
Plasma Processing Laboratory, Department of Chemical and Biomolecular Engineering, University of Houston, Houston, Texas 77204-4004, USA

(Received 2 April 2014; accepted 6 June 2014; published online 19 June 2014)

A kinetic Particle-In-Cell simulation with Monte Carlo Collisions was performed of a geometrically symmetric capacitively coupled, parallel-plate discharge in argon, driven by trapezoidal asymmetric voltage pulses with a period of 200 ns. The discharge was electrically asymmetric, making the ion energy distributions at the two electrodes different from one another. The fraction of the period (α), during which the voltage was kept at a constant (top-flat) positive value, was a critical control parameter. For the parameter range investigated, as α increased, the mean ion energy on the grounded electrode increased and the ions became more directional, whereas the opposite was found for the ions striking the powered electrode. The absolute value of the DC self-bias voltage decreased as α increased. Plasma instabilities, promoted by local double layers and electric field reversals during the time of the positive voltage excursion, were characterized by electron plasma waves launched from the sheath edge. © *2014 AIP Publishing LLC*. [http://dx.doi.org/10.1063/1.4884017]

I. INTRODUCTION

Control of the energy and angular distributions of ions bombarding a substrate in contact with plasma is of paramount importance for plasma processing.[1] For example, the ion bombardment energy is critical for controlling film microstructure and properties in plasma enhanced chemical vapor deposition (PECVD). The large area parallel plate capacitively coupled reactors used for PECVD are almost geometrically symmetric, i.e., the areas of the radio frequency (RF) powered and grounded electrodes are almost identical. The deposition rate can be increased by increasing RF power but, for the classical sinusoidal voltage, the concomitant increase in ion energy can degrade the quality of the deposited film. In etching reactors, both the direction and the energy distribution of the ions bombarding the substrate are essential. Ions perpendicular to the substrate are required to obtain anisotropic etching. In addition, the ion energy must be high enough to promote etching, but not too high to cause sputtering, substrate damage, or loss of selectivity with respect to the mask or the underlying layer. As device dimensions approach atomic level, precise control of the ion energy distribution (IED) (not just the average ion energy) becomes critical.[2]

The energy of ions bombarding the substrate depends on the sheath voltage, which in turn is controlled by the applied voltage waveform. For sinusoidal sheath voltage and collisionless sheath, the IED is bimodal.[3–5] The controlling parameter is $\frac{\tau_i}{\tau_{rf}} = \frac{3s\omega}{2\pi}\left(\frac{M}{2\,\mathrm{eV}_{sh}}\right)^{1/2}$ the ratio of the ion transit time through the sheath to the period of the applied RF.[1–3] Here, s, ω, M, and V_{sh} are time-averaged sheath thickness, applied field angular frequency, ion mass, and time-average sheath voltage, respectively. When $\tau_i/\tau_{RF} \ll 1$, ions respond to the instantaneous sheath voltage, and the IED has a large energy spread. When $\tau_i/\tau_{RF} \gg 1$, ions respond to a time-averaged sheath voltage, and the IED narrows. The width of the distribution may be decreased by increasing the frequency of the applied field, which increases τ_i/τ_{RF}. However, when the frequency becomes too high, the RF wavelength becomes comparable to the substrate dimension, resulting in non-uniform voltage distribution across the substrate. In the presence of ion-neutral charge exchange collisions in the sheath, the IED exhibits multiple peaks.[6]

The IED may be controlled by applying a tailored voltage waveform on the substrate electrode. Barnat *et al.*[7–9] used trapezoidal asymmetric voltage pulses, whereby charging of dielectric substrates was minimized by shortening the pulse duration. Wendt and co-workers[10–13] applied a low frequency impulse waveform or a staircase waveform on a substrate immersed in a continuous wave (CW) plasma to obtain a peaked IED. The waveform had to be given the right slope to account for charging of non-conductive substrates, and still yield a nearly constant sheath potential, and thus a nearly monoenergetic IED, in the limit $\tau_i/\tau_{RF} \ll 1$. A similar approach was taken in Refs. 14–16, where the authors also studied the influence of substrate charging on the required voltage waveform, so that monoenergetic IEDs may be obtained. Agarwal and Kushner[17] and Rauf[18] conducted computational investigations of the effect of non-sinusoidal bias voltage waveforms on the IED, etching rate, and selectivity. In all these studies, the plasma was generated by independent means (for example, inductively coupled plasma (ICP)), and the voltage waveform was applied to a separate electrode holding the substrate.

Other investigators have studied systems where a tailored voltage waveform powers the plasma, and at the same time controls the IED. In particular, the Electrical Asymmetry Effect (EAE)[19] provides a way of controlling the IED by applying a plasma sustaining voltage of the form, $V(t) = U_1\cos(2\pi f_1 t + \theta_1) + U_2\cos(2\pi f_2 t)$ to one of the electrodes

[a]padiomede@gmail.com
[b]economou@uh.edu

of an otherwise "standard" capacitively coupled plasma (CCP) reactor (the other electrode is grounded), with $f_2 = 2f_1$. By changing the phase angle θ_1 between the two driving frequencies, one can shift (almost linearly) the resulting DC self-bias voltage and therefore the ion energy. Importantly, the ion energy can be varied while keeping a constant ion flux. A DC self-bias is generated, even in systems with electrodes of equal area, if the applied waveform is asymmetric, i.e., the amplitude of the positive swing of the waveform is different than the amplitude of the negative swing. One can utilize more harmonics to enhance the EAE but practical implementation becomes cumbersome. The authors of Refs. 20–22 applied Gaussian pulses (or similar waveforms with multiple harmonics) and showed that the ion flux could be increased while the average ion energy did not change appreciably. Also, it was possible to swap the role of electrodes by switching the waveform from "peaks" to "valleys."

In this work, the EAE resulting by the application of trapezoidal asymmetric voltage pulses to an electrode of a geometrically symmetric parallel-plate CCP was studied by a particle-in-cell simulation with Monte Carlo collisions (PIC-MCC). In contrast to previous studies, in which the plasma was sustained by an independent power supply,[9,17,18] the voltage waveform in this work was also the plasma sustaining voltage.

II. SIMULATION

Simulations were performed using a purposely modified version of XPDP1[23,24] a one-dimensional PIC-MCC code. A geometrically symmetric (equal electrode areas), capacitively coupled parallel-plate (plate separation 6 cm) argon plasma was simulated assuming a uniform background gas density of $1.9 \times 10^{20}\,m^{-3}$ (corresponding to 10 mTorr at 500 K). A tailored voltage waveform was applied to one of the electrodes of the CCP reactor through a blocking capacitor (fixed at $10\,nF/m^2$), while the other electrode was grounded (Fig. 1). A cycle (period of 200 ns) of the applied waveform consisted of a negative constant DC voltage followed by a brief excursion to a positive DC voltage, with specified ramp-up and ramp-down times (Fig. 2). For this work, the ramp-up and

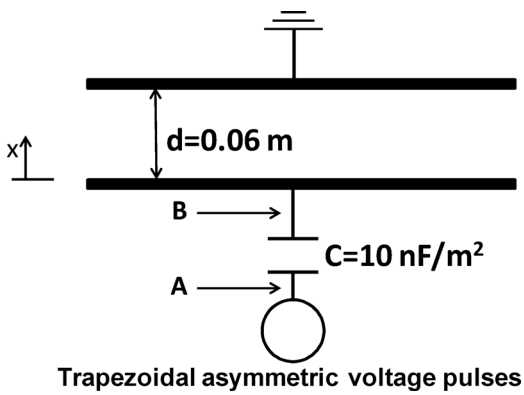

FIG. 1. Schematic of the reactor used for simulations. Trapezoidal asymmetric voltage pulses were applied to an electrode of a geometrically symmetric parallel-plate capacitively coupled plasma reactor through a blocking capacitor. The counter electrode was grounded. Voltage was applied at point A. The resulting substrate electrode (assumed conductive) voltage was that at point B.

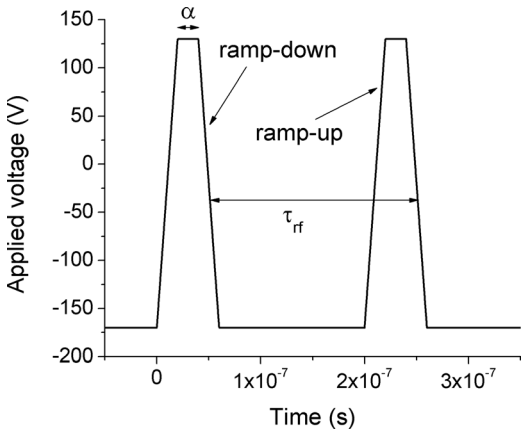

FIG. 2. Applied trapezoidal asymmetric voltage pulse waveform (not to scale), characterized by α, the fraction of the period with a constant positive voltage (flat-top), and by ramp-up and ramp-down times (4 ns each). The frequency of the waveform for the base case was 5 MHz (period $\tau_{RF} = 200$ ns).

ramp-down times were fixed at 0.02 of the period (i.e., 4 ns each). The waveform was characterized by parameter α, the fraction of the cycle spent at constant (top-flat) positive voltage. The negative DC voltage controls the ion energy. During application of this voltage, the electrode is bombarded by positive ions; electrons cannot overcome the large sheath potential to reach the electrode. However, due to the presence of the capacitor, positive charge accumulates on the electrode. The brief excursion to positive DC is necessary to attract a burst of electrons and neutralize the accumulated positive charge. The applied trapezoidal pulses (with a frequency of 5 MHz) were asymmetric, i.e., the absolute value of the negative peak DC voltage (−170 V) was different from the positive peak DC voltage (130 V). Because of the asymmetry of the applied voltage, the discharge was electrically asymmetric (EAE[19]) with a DC self-bias developing despite the fact that both the powered and the grounded electrodes were of the same geometrical area. Singly charged argon positive ions and electrons were considered in the simulation. Electron elastic scattering, excitation and ionization, as well as ion–neutral collisions (both scattering and charge exchange) were included.[25] The common restrictions on time step and grid size of the PIC simulation were observed.[26] The standard leap frog scheme was used to advance particles,[26] and the null collision method was used for Monte Carlo collisions.[25] Electron-electron collisions were not important under the relatively low electron densities examined. The secondary electron emission coefficient due to ion bombardment of the electrodes was set to 0.02. Also, metastable argon atoms do not influence the discharge at the low pressure considered. The simulation ran until steady-state, which typically took ~1000 rf cycles. By doubling the number of cycles, the charged particle number densities and the voltage waveform at the powered electrode changed less than 0.1%.

III. RESULTS AND DISCUSSION

A. Base case conditions

Fig. 3(a) shows the time-averaged potential distribution in the interelectrode gap obtained for the base case

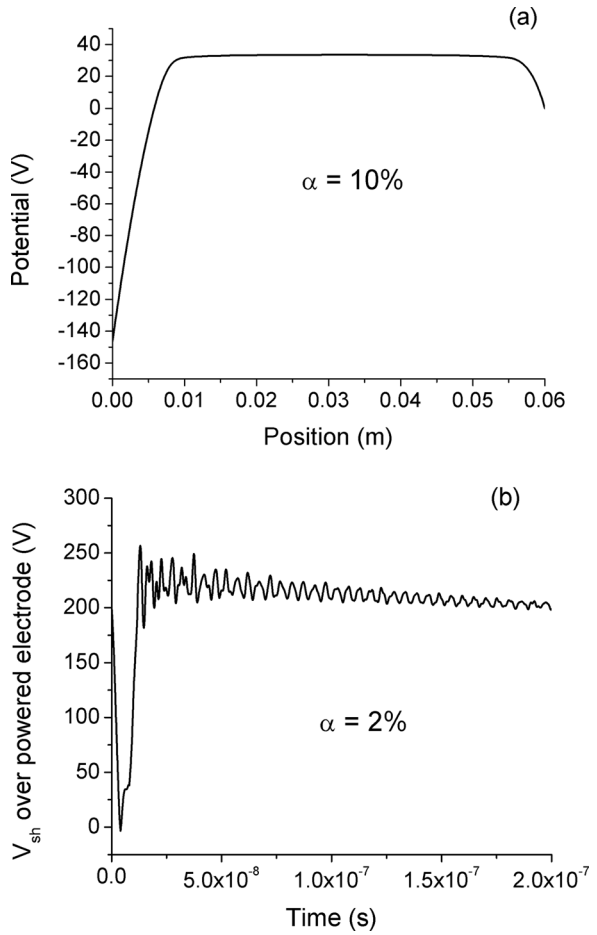

FIG. 3. (a) Time-average potential distribution in the interelectrode gap for the base case conditions (Table I). The powered electrode was at $x = 0$. (b) Time dependence of the powered sheath voltage during a pulse, for $\alpha = 2\%$. Other conditions were at the base case values (Table I).

parameters shown in Table I. The electrical asymmetry of the plasma is evident, resulting in a DC self-bias voltage of $V_{dc} = -146$ V. This is due to the asymmetry of the applied voltage.[19] Application of a sinusoidal waveform would have resulted in a DC self-bias of zero, for this geometrically symmetric system. For the voltage waveform considered in this study, the voltage drop across the powered electrode sheath is larger than that across the grounded electrode sheath. The time-averaged plasma potential at the center of the gap ($x = 3$ cm) is $V_p = 33.6$ V. Thus, the time-averaged sheath voltage over the powered electrode is approximately equal to $|V_{dc}| + V_p \sim 180$ V.

TABLE I. Base case parameter values.

Ar gas pressure	10 mTorr
Gas temperature	500 K
Interelectrode gap	0.06 m
Frequency of applied waveform	5 MHz
Ramp-up time	4 ns
Ramp-down time	4 ns
Peak positive DC voltage	130 V
Peak negative DC voltage	−170 V
α,fraction of period at constant positive voltage	10%

For a typical time-averaged powered electrode sheath thickness of 0.01 m, and a sheath voltage of ~180 V, the ion (Ar^+) transit time through a collisionless sheath is $\tau_i = 3s[M/(2\,eV_s)]^{1/2} \sim 1\ \mu$s, much larger than 28 ns, the duration of the pulse of the applied waveform for $\alpha = 10\%$ (including 4 ns of ramp-up and 4 ns of ramp-down). Therefore, ions do not "see" the positive DC excursion for small α, and the sheath potential variation due to this excursion should not contribute significantly to broadening the full width at half maximum (FWHM) of the IED. However, for large values of α, the ion transit time is no longer much larger than the duration of the positive DC pulse of the applied waveform and the contribution of this pulse to the FWHM of the IED may become significant.

The time dependence of the voltage of the sheath over the powered electrode is shown in Fig. 3(b). The high frequency oscillations are due to a plasma instability that will be discussed in Sec. III C. The sheath voltage collapses to around zero for a brief time during the period, allowing electrons to rush to the electrode and neutralize the positive charge that has accumulated on the electrode during the period. Ions can follow neither the collapse nor the re-establishment of the sheath voltage during the positive pulse of the applied waveform. However, due to capacitor charging, there is a significant sheath voltage variation (~25 V) over the time scale (200 ns) of the period of the applied waveform. Since ions can respond (at least partially) on this time scale, such voltage variation is a significant contributor to broadening of the IED. Ions cannot respond to the high frequency oscillations of the sheath voltage.

The ion energies on the powered (Fig. 4(a)) and grounded (Fig. 4(b)) electrodes reflect the sheath voltages, with ions striking the powered electrode being more energetic than those at the grounded electrode. The IED on the powered electrode is a characteristic bimodal centered on the time-averaged sheath voltage (~180 V). The tail of the IED to the left of the main feature is due to ion-neutral collisions. Under these conditions, the ion mean free path $\lambda_i = 1/(N\sigma) \sim 0.01$ m (the charge exchange collision cross section for argon is $\sigma \sim 5 \times 10^{-19}$ m^2 and the neutral gas density is $N = 1.9 \times 10^{20}$ m^{-3}), commensurate with the time-averaged sheath width of $s \sim 0.01$ m. The weak peaks in the tail of the IED are due to the creation of cold ions by symmetric charge exchange collisions of fast Ar^+ ions with cold Ar neutrals, combined with RF modulation of the sheath electric field (see p. 446 of Ref. 1). The FWHM of the IED is a result of three mechanisms: (a) capacitor charging during a period, resulting in variation of the sheath potential with time (Fig. 3(b)), (b) RF modulation of the sheath width, and (c) ion-neutral collisions in the sheath. Of these, charging appears to be the dominant mechanism controlling the width of the IED. Similar features are observed in the IED on the grounded electrode (Fig. 4(b)): a bimodal distribution centered on the time-averaged sheath voltage (in this case the time-averaged plasma potential), with a tail due to collisions. The weak peaks in the tail are again due to symmetric charge exchange collisions.

Figs. 5 and 6 show the spatial evolution of the IED in the powered and grounded sheaths. In each panel, the

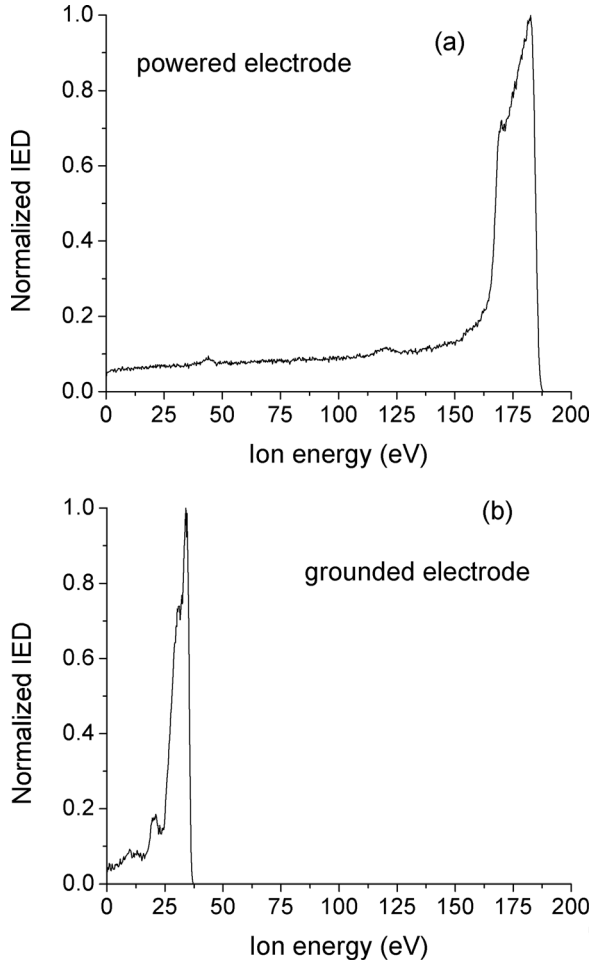

FIG. 4. Ion energy distributions at the powered (a), and grounded (b) electrodes for the base case conditions (Table I).

distance from the powered electrode (which is located at $x = 0$) is given. At the edge of the sheath over the powered electrode (a distance of 0.012 m from that electrode), the IED is fairly sharp with a FWHM of $\sim T_e$ (Fig. 5(a)). This reflects the acceleration of ions in the presheath.[27,28] As ions move closer to the electrode, the IED shifts to higher energies and its FWHM widens because of the varying sheath potential (Fig. 3(b)), due to charging, aided by occasional collisions, and the RF oscillations of the field. The IED is widest at the electrode surface. A similar evolution of the IED is observed in the sheath over the grounded electrode except for the lower sheath voltage and concomitantly lower ion energy (note the expanded x-axis scale of Fig. 6 compared to Fig. 5).

B. Effect of α

Fig. 7 shows the DC self-bias voltage as a function of α. As α increases, the DC self-bias voltage becomes less negative, as the waveform becomes less asymmetric. Figs. 8 and 9 show the IEDs at the grounded and powered electrodes, respectively, for different values of α. At the grounded electrode, the maximum ion energy increases with α, because the plasma potential also increases with α (the system becomes less asymmetric). The bimodal part of the distribution

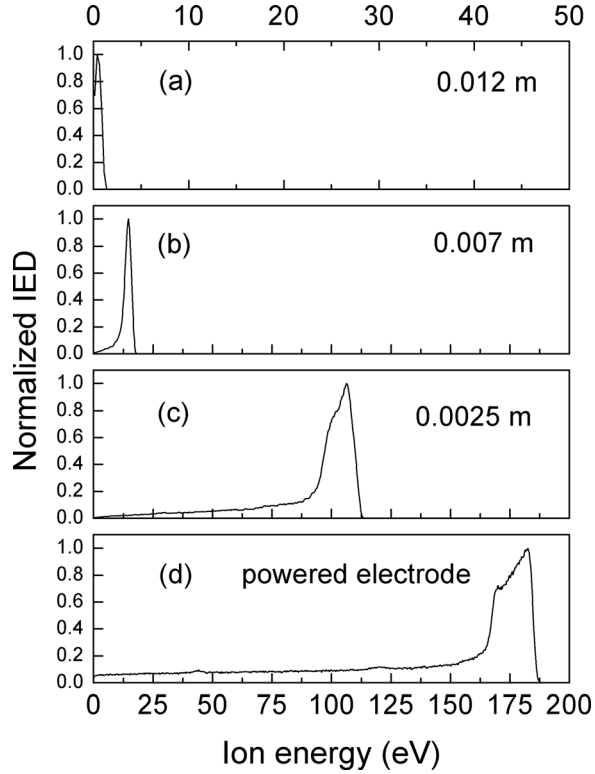

FIG. 5. Spatial evolution of the ion energy distribution in the sheath over the powered electrode, for the base case conditions (Table I). Distance from the powered electrode: (a) 0.012 m (∼sheath edge), (b) 0.007 m, (c) 0.0025 m, (d) 0.0, i.e., at the powered electrode.

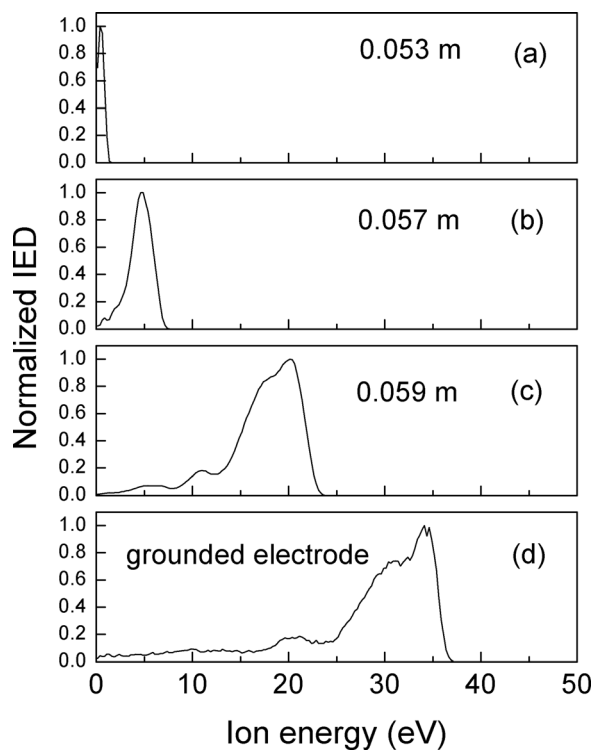

FIG. 6. Spatial evolution of the ion energy distribution in the sheath over the grounded electrode, for the base case conditions (Table I). Distance from the *powered* electrode: (a) 0.053 m (∼sheath edge), (b) 0.057 m, (c) 0.059 m, (d) 0.060 m, i.e., at the grounded electrode.

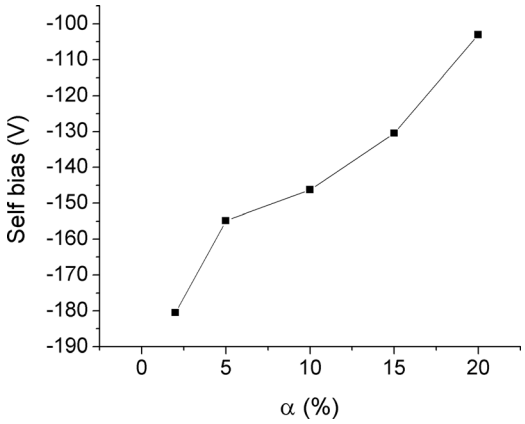

FIG. 7. DC self-bias voltage as a function of α, the fraction of the period with a constant positive voltage. Other conditions were as in Table I.

becomes wider, and the tail is enhanced due to higher probability of ion-neutral collisions in the sheath, as α increases. The ion sheath transit time scales with the sheath thickness (s) and the time-averaged sheath voltage (V_{sh}) according to $\tau_i \sim sV_{sh}^{-0.5}$ (Eq. 2 of Ref. 3) while s scales as $s \sim V_{sh}^{0.75}$ (Ref. 1, p. 177). Thus, the ion transit time has a weak dependence on the sheath voltage ($\tau_i \sim V_{sh}^{0.25}$), and it is not the cause of the IED widening with increasing α. If the value of α is small enough, ions do not respond to the change in the sheath potential during application of the positive voltage pulse, and the perturbation of the narrow IED is small. This is reflected in the sharper IEDs for smaller values of α (Figs. 8 and 9). The ion angular distribution (not shown) on the grounded electrode was approximately Gaussian with FWHM in the range of 3.2°–4.4°, depending on α. Ions struck the grounded electrode with a tighter angular

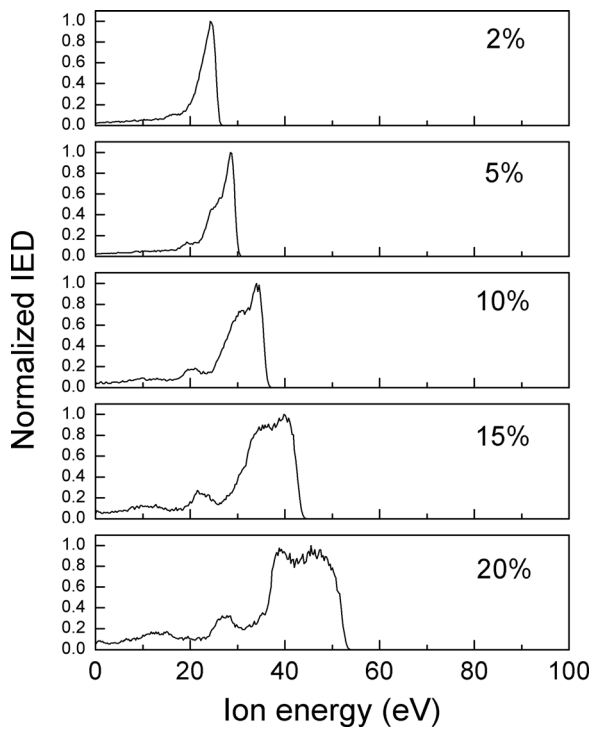

FIG. 8. Ion energy distribution at the grounded electrode for different values of α, the fraction of the period with a constant positive voltage. Other conditions were as in Table I.

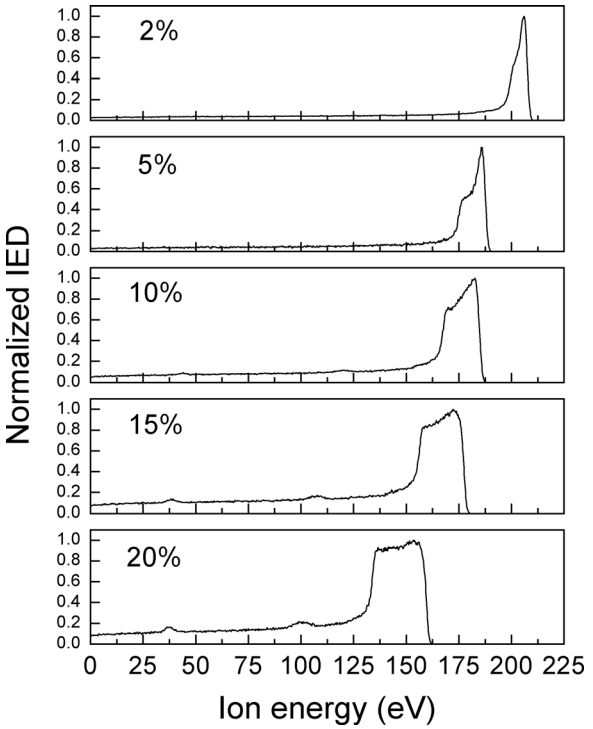

FIG. 9. Ion energy distribution at the powered electrode for different values of α, the fraction of the period with a constant positive voltage. Other conditions were as in Table I.

distribution as α increased, because of the higher directional velocity of ions.

At the powered electrode, the maximum ion energy decreases with α, following the trend of the DC self-bias, while the bimodal part of the distribution becomes wider and the collision-induced tail is enhanced, similar to the grounded electrode. Also, the ion directionality (not shown) became a little worse (FWHM range of 1.6°–1.8°) as α increased, due to the decrease in the directional velocity of ions. The variation with α of the DC self-bias and the maximum ion energy at the powered electrode are different compared to Ref. 17 due to the geometrical asymmetry of the reactor simulated in Ref. 17, and the fact that, in contrast to the present work, the plasma was sustained by an ICP source independently from the substrate bias voltage source.

When the frequency of the applied voltage waveform was increased from 5 MHz to 10 MHz (other conditions at base case), the peak plasma density increased from 4.3×10^{15} to $1.8 \times 10^{16}\,m^{-3}$ following the ω^2 scaling of electron density with excitation frequency.[1] This resulted in thinner sheaths, shorter ion transit time through the sheath, and smaller ion-neutral collision probability. This in turn produced narrower bimodal IEDs and a less pronounced tail to the left of the main peak for both the powered and grounded electrodes.

C. Plasma instability

The response time of electrons is the electron plasma frequency which, for the conditions of this study, is at least 200 MHz, corresponding to the electron density near the plasma-sheath interface. Thus, electrons respond to the

variations of the sheath voltage, but some electron inertia may still persist. When the applied voltage waveform swings towards positive values (ramp-up) the sheath voltage decreases (Fig. 3(b)), and electrons are attracted to the powered electrode, only to be pushed back into the plasma when the applied voltage turns towards negative values (ramp-down) and the sheath voltage increases. This violent expansion and compression of the electron cloud give rise to a plasma instability accompanied by the formation of double layers (formed by electron overshooting their positions due to inertia), and electric field reversals near the sheath edge. The electron conduction current at the plasma center ($x = 3$ cm) is displayed in Fig. 10, along with the voltage waveform appearing on the powered electrode (point B of Fig. 1). The corresponding sheath potential is shown in Fig. 3(b). The oscillations of the electron current are damped with time within a pulse period. The amplitude of the oscillations of the current was found to become smaller when α was increased from 2% to 10% (not shown).

Fig. 11 shows important plasma characteristics in the sheath region ($x = 0$ to 2 cm) of the powered electrode for $\alpha = 2\%$. Time $t = 0$ corresponds to the start of the ramp towards the positive swing of the voltage (see Fig. 2). During this ramp-up, electrons are attracted to the powered electrode (located at $x = 0$) and, as the voltage returns to its peak negative value, a beam of energetic electrons is pushed back into the plasma bulk, generating an instability at time $t \sim 12$ ns. Fig. 11(a) shows the formation of double layers (alternating net positive and negative charge) at the sheath edge. As a consequence, modulation of the space potential (Fig. 11(b)) and field reversals (Fig. 11(c)) occur.

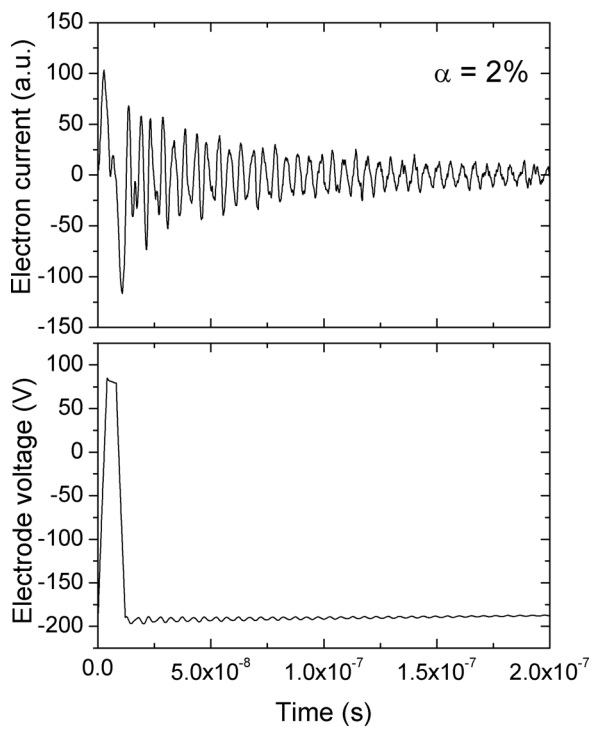

FIG. 10. (top) Electron conduction current at the discharge center, and (bottom) voltage at the powered electrode (at point B of Fig. 1), as a function of time during one RF cycle. The value of α was 2%. Other conditions were as in Table I.

(In a field reversal, the electric field is pointing towards the bulk plasma.) Compression of the electron fluid during sheath expansion (ramp-down) gives rise to a wave propagating into the bulk plasma. The electron density is oscillatory, especially at the sheath edge (Fig. 11(d)). The frequency of the oscillations is 224 MHz, almost exactly equal to the electron plasma frequency at the sheath edge (220 MHz). Thus, these oscillations constitute electron plasma waves propagating towards the bulk plasma. Such waves can contribute to collisionless electron heating by Landau damping or other electron-wave interactions. Electron-neutral collisions dampen these waves as was found by simulations at higher pressures. Also, the instability was found to become less pronounced when α was increased between 2% and 10%.

Electron plasma waves were observed by Sharma and Turner[29] in a semi-infinite plasma with an applied sinusoidal current waveform, for relatively high current densities. Such waves appear to be of the same origin as those reported in the present work. The authors also observed field reversal and periodic double layer structures at the sheath edge and attributed the emission of waves to trapping and release of electrons from the potential wells formed by the electric field reversals. However, they could not capture bounce back of electrons from the opposite sheath (see next paragraph) since they considered a semi-infinite plasma (one sheath only).

Enhanced understanding of the instability may be obtained by looking at v_x-x phase-space plots of electrons. Fig. 12 shows snapshots at different times during the instability for $\alpha = 2\%$. For reference, the voltage pulse starts at $t = 0$, ramps-up until $t = 4$ ns, then stays at a constant positive value (top-flat) until $t = 8$ ns, when it begins to ramp-down ending at $t = 12$ ns. At $t = 6$ ns, a bunch of electrons is attracted to the powered electrode by the positive voltage and, while this voltage is reaching its peak negative value (at time $t \sim 12$ ns), the electron beam is pushed back into the plasma bulk, commencing the instability. Several secondary streams of electrons are launched from the sheath edge and move back and forth between the powered and grounded sheaths, until the instability is damped.

The electron energy probability function (EEPF) at the powered sheath edge for different times is plotted in Fig. 13(a), for $\alpha = 2\%$. When the voltage ramps-up and is positive, the distribution is a low temperature Maxwellian. When the instability starts (at 12 ns), the EEPF becomes bi-Maxwellian with a high energy (up to about 100 eV) tail, and heating is retained several ns after the onset of the instability. For $\alpha = 10\%$ (Fig. 13(b)), the energy distribution is already bi-Maxwellian before the voltage returns to ramp-down, because of the electron wave generated during the previous pulse. When the voltage becomes negative, there is still some heating of the distribution, but it is not as effective as in the $\alpha = 2\%$ case, and the EEPF tail cools down faster. In a study by Sun *et al.*,[30] the authors applied periodically a very strong negative DC pulse (−2500 V) to the powered electrode of an otherwise conventional RF excited CCP. They observed not only heating of the EEDF but also an increase in plasma density.

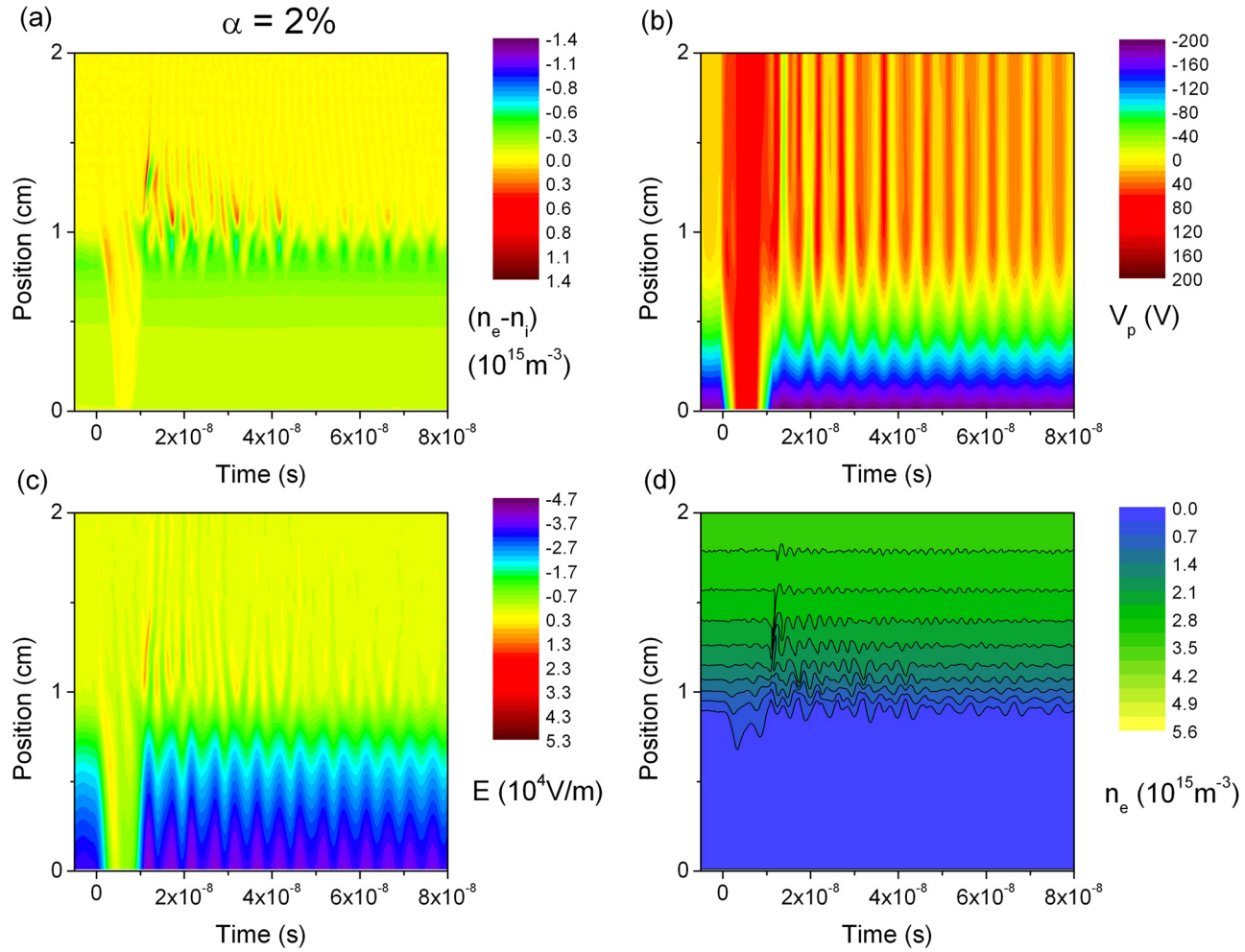

FIG. 11. Spatiotemporal profiles of plasma characteristics in the sheath region ($x = 0$–2 cm) next to the powered electrode, located at $x = 0$: (a) net charge density (n_e-n_i), (b) electric potential, (c) electric field, and (d) electron number density. The value of α was 2%. Other conditions were as in Table I. Time $t = 0$ corresponds to the start of the pulse (see Fig. 2).

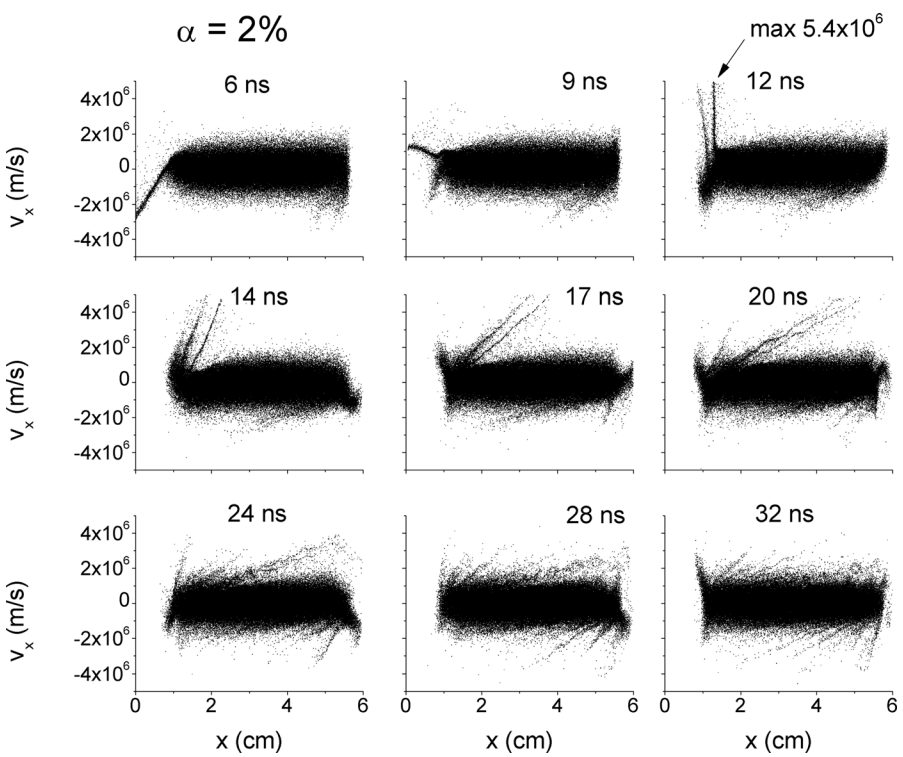

FIG. 12. v_x-x phase-space of electrons for different times around the onset of the instability. The applied voltage pulse started at $t = 0$ and ended at $t = 12$ ns (see Fig. 2). The value of α was 2%. Other conditions were as in Table I. The powered electrode was at position $x = 0$ and the grounded electrode was at $x = 6$ cm. The maximum x-component of the electron velocity (v_x) was 5.4×10^6 m/s.

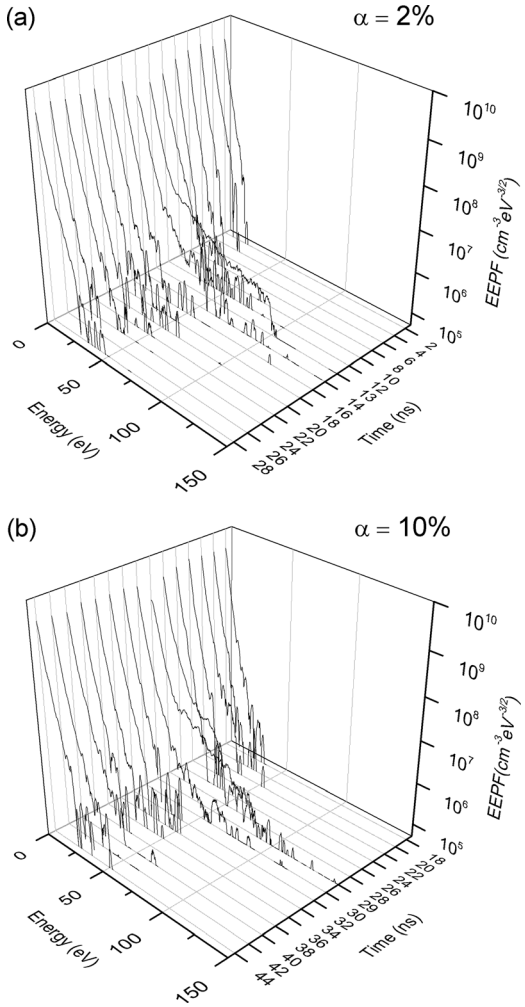

FIG. 13. EEPF at the powered electrode sheath edge for times around the onset of the instability: (a) the positive swing of the applied voltage pulse started at $t = 0$ and ended at $t = 12$ ns ($\alpha = 2\%$). (b) The positive swing of the applied voltage pulse started at $t = 0$ and ended at t = 28 ns ($\alpha = 10\%$). Other conditions were as in Table I.

D. Charging effects

When the substrate electrode is covered by a dielectric, the capacitance of this dielectric, as well as any stray capacitance, can be combined with that of the blocking capacitor. Also, in practical systems, the electrostatic chuck presents a capacitance that should be accounted for. In any case, the equivalent capacitor will charge-up to a voltage given by $dV/dt = (1/C)\ dq/dt$, where C is the total (equivalent) capacitance per unit area and q is the net charge per unit area arriving from the plasma due to ion and/or electron bombardment. When the applied voltage waveform is at its peak negative value, the substrate is bombarded by positive ions only, and $dq/dt = I_i$, the ion current density. The positive ion current density for $\alpha = 2\%$ is 0.24 A/m^2, and the capacitance is 10 nF/m^2.Then, the rate of change of the powered electrode voltage is found from the above relation to be 0.024 V/ns. For a negative DC peak voltage lasting 188 ns, the resulting charge-up voltage will be 4.5 V, close to ~5 V differential of the time-average voltage between $t = 12$ ns and $t = 200$ ns found by simulation (Fig. 10 (bottom)). Assuming that this charging voltage (and the resulting broadening of the IED) can be tolerated, it is not necessary to make the plateau negative voltage of the applied waveform more negative as a function of time (non-zero slope), to compensate for the effect of charging, in order to maintain a constant sheath voltage, to achieve a nearly monoenergetic IED.[12,14]

IV. SUMMARY

A kinetic PIC-MCC was performed to investigate the application of trapezoidal asymmetric voltage pulses to one of the electrodes of a parallel-plate capacitively coupled plasma reactor, with a grounded counter-electrode. Application of such pulses produced electrical asymmetry, and a DC self-bias despite the geometrical symmetry (equal electrode areas) of the reactor. The IED could be controlled by controlling α, the fraction of the period with a constant positive voltage. As α increased, the applied waveform became less asymmetric and the DC self-bias voltage became less negative. Also, as α increased, the mean ion energy at the grounded electrode increased and the ions became more directional, while the opposite occurred for the ions striking the powered electrode. A beam-plasma instability was generated by electrons pulled to the powered electrode, and then suddenly pushed back into the bulk plasma during positive swing of the voltage pulse. Electron plasma waves launched from the sheath edge were characterized by the formation of double layers and local electric field reversals. Such waves can contribute to collisionless electron heating by Landau damping or other electron-wave interactions. The evolution of the IED as a function of position from the electrodes was also studied. For very small α, the main broadening mechanism of the IED was the sheath voltage variation due to charging of the blocking capacitor.

Unfortunately, no experimental data could be found on the system studied. Thus, comparison of the simulation predictions with experiment is yet to be performed.

ACKNOWLEDGMENTS

Financial support for this work, provided by the Department of Energy, Office of Fusion Energy Science, Contract No. DE-SC0001939, and the National Science Foundation Grant Nos. CMMI-1030620 and IIP-1343387, is gratefully acknowledged.

[1]M. A. Lieberman and A. J. Lichtenberg, *Principles of Plasma Discharges and Materials Processing*, 2nd ed. (Wiley, Hoboken, NJ, 2005).
[2]D. J. Economou, J. Vac. Sci. Technol. A **31**, 050823 (2013).
[3]E. Kawamura, V. Vahedi, M. A. Lieberman, and C. K. Birdsall, Plasma Sources Sci. Technol. **8**, R45 (1999).
[4]T. Panagopoulos and D. J. Economou, J. Appl. Phys. **85**, 3435 (1999).
[5]E. A. Edelberg and E. S. Aydil, J. Appl. Phys. **86**, 4799 (1999).
[6]C. Wild and P. Koidl, Appl. Phys. Lett. **54**, 505 (1989).
[7]E. V. Barnat and T.-M. Lu, J. Vac. Sci. Technol. A **17**, 3322 (1999).
[8]E. V. Barnat and T.-M. Lu, Phys. Rev. E **66**, 056401 (2002).
[9]E. V. Barnat and T.-M. Lu, J. Appl. Phys. **92**, 2984 (2002).
[10]X. V. Qin, Y.-H. Ting, and A. E. Wendt, Plasma Sources Sci. Technol. **19**, 065014 (2010).
[11]M. M. Patterson, H.-Y. Chu, and A. E. Wendt, Plasma Sources Sci. Technol. **16**, 257 (2007).
[12]S.-B. Wang and A. E. Wendt, J. Appl. Phys. **88**, 643 (2000).
[13]F. L. Buzzi, Y.-H. Ting, and A. E. Wendt, Plasma Sources Sci. Technol. **18**, 025009 (2009).

[14]P. Kudlacek, R. F. Rumphorst, and M. C. M. van de Sanden, J. Appl. Phys. **106**, 073303 (2009).
[15]I. T. Martin, M. A. Wank, M. A. Blauw, R. A. C. M. M. van Swaaij, W. M. M. Kessels, and M. C. M. van de Sanden, Plasma Sources Sci. Technol. **19**, 015012 (2010).
[16]M. A. Wank, R. A. C. M. M. van Swaaij, P. Kudlacek, M. C. M. van de Sanden, and M. Zeman, J. Appl. Phys. **108**, 103304 (2010).
[17]A. Agarwal and M. J. Kushner, J. Vac. Sci. Technol. A **23**, 1440 (2005).
[18]S. Rauf, J. Appl. Phys. **87**, 7647 (2000).
[19]U. Czarnetzki, J. Schulze, E. Schüngel, and Z. Donkó, Plasma Sources Sci. Technol. **20**, 024010 (2011).
[20]T. Lafleur and J. P. Booth, J. Phys. D: Appl. Phys. **45**, 395203 (2012).
[21]T. Lafleur, P. A. Delattre, E. V. Johnson, and J. P. Booth, Appl. Phys. Lett. **101**, 124104 (2012).
[22]P. A. Delattre, T. Lafleur, E. V. Johnson, and J. P. Booth, J. Phys. D: Appl. Phys. **46**, 235201 (2013).
[23]V. Vahedi, G. DiPeso, C. K. Birdsall, M. A. Lieberman, and T. D. Rognlien, Plasma Sources Sci. Technol. **2**, 261 (1993).
[24]J. P. Verboncoeur, M. V. Alves, V. Vahedi, and C. K. Birdsall, J. Comput. Phys. **104**, 321 (1993).
[25]V. Vahedi and M. Surendra, Comput. Phys. Commun. **87**, 179 (1995).
[26]C. K. Birdsall and A. B. Langdon, *Plasma Physics via Computer Simulation* (McGraw-Hill, New York, 1985).
[27]K.-U. Riemann, J. Phys. D: Appl. Phys. **36**, 2811 (2003).
[28]U. Kortshagen and M. Zethoff, Plasma Sources Sci. Technol. **4**, 541 (1995).
[29]S. Sharma and M. M. Turner, Phys. Plasmas **20**, 073507 (2013).
[30]J. Sun, X. Li, C. Sang, W. Jiang, P. Zhang, and D. Wang, Phys. Plasmas **17**, 103505 (2010).